(Title) Altered Fhod3 Expression Involved in Progressive High-Frequency Hearing Loss via Dysregulation of Actin Polymerization Stoichiometry in The Cuticular Plate

Ely Cheikh Boussaty[1]*, Yuzuru Ninoyu[1]*, Leo Andrade[2], Qingzhong Li[3], Ryu Takeya[4], Hideki Sumimoto[5], Takahiro Ohyama[3], Karl J Wahlin[6], Uri Manor[2,7]†, Rick A Friedman[1]†

1. Department of Otolaryngology – Head and Neck Surgery, University of California, San Diego, La Jolla, CA, USA
2. Waitt Advanced Biophotonics Center, Salk Institute for Biological Studies, La Jolla, CA, USA
3. USC-Tina and Rick Caruso Department of Otolaryngology-Head & Neck Surgery, Zilkha Neurogenetic Institute, USC Keck School of Medicine, University of Southern California, Los Angeles, USA
4. Department of Pharmacology, Faculty of Medicine, University of Miyazaki, Miyazaki, Japan
5. Department of Biochemistry, Kyushu University Graduate School of Medical Sciences, Fukuoka, Japan
6. Shiley Eye Institute, University of California, San Diego, San Diego, CA, USA
7. Department of Cell & Developmental Biology, School of Biological Sciences, University of California, San Diego, USA

* These authors contributed equally to this work.

† Corresponding author:

Rick A Friedman (rafriedman@health.ucsd.edu), Uri Manor(urimanor@ucsd.edu)

Running title: Fhod3 regulates actin dynamics in the cochlea

Keywords: Age-related hearing loss (ARHL), Genome-wide association studies (GWAS), hair cells, actin, stereocilia, Multiplexed error-robust fluorescence in situ hybridization (MERFISH)

Number of figures: 5

Abstract

Age-related hearing loss (ARHL) is a common sensory impairment with complex underlying mechanisms. In our previous study, we performed a meta-analysis of genome-wide association studies (GWAS) in mice and identified a novel locus on chromosome 18 associated with ARHL specifically linked to a 32 kHz tone burst stimulus. Consequently, we investigated the role of Formin Homology 2 Domain Containing 3 (Fhod3), a newly discovered candidate gene for ARHL based on the GWAS results. We observed Fhod3 expression in auditory hair cells (HCs) and primarily localized at the cuticular plate (CP). To understand the functional implications of Fhod3 in the cochlea, we generated Fhod3 overexpression mice (*Pax2-Cre*$^{+/-}$*; Fhod3*$^{Tg/+}$) (TG) and HC-specific conditional knockout mice (*Atoh1-Cre*$^{+/-}$*; Fhod3*$^{fl/fl}$) (KO). Audiological assessments in TG mice demonstrated progressive high-frequency hearing loss, characterized by predominant loss of outer hair cells, and a decreased phalloidin intensities of CP. Ultrastructural analysis revealed shortened stereocilia in the basal turn cochlea. Importantly, the hearing and HC phenotype in TG mice were replicated in KO mice. These findings indicate that Fhod3 plays a critical role in regulating actin dynamics in CP and stereocilia. Further investigation of Fhod3 related hearing impairment mechanisms may facilitate the development of therapeutic strategies for ARHL in humans.

1 Introduction

Age-related hearing loss (ARHL) is one of the most common causes of sensorineural hearing loss among elderly population. Numerous studies have identified candidate genes associated with ARHL, implicating cellular pathways such as oxidative stress response (Sugiura et al. 2010; Someya et al. 2010), inflammation (Rodríguez-de la Rosa et al. 2017; Menardo et al. 2012), and cellular senescence (Benkafadar et al. 2019; Li et al. 2022). However, with the polygenic

56 nature (Fransen et al. 2015) and phenotypic heterogeneity of ARHL (Gates and Mills 2005), the
57 underlying mechanisms have not been fully elucidated. Further investigation is necessary to
58 facilitate targeted interventions and personalized treatment approaches for ARHL.
59 Genome-wide association studies (GWAS) have been conducted in humans to explore the genetic
60 architecture of ARHL and have successfully identified loci associated with susceptibility to ARHL
61 (Friedman et al. 2009; Van Laer et al. 2010). However, GWAS studies often explain only a fraction
62 of the heritability of complex traits, which imply the presence of undiscovered genetic variants
63 contributing to ARHL. This may be attributed to limitations in study design, sample size, or the
64 influence of rare variants that are challenging to detect. To address these challenges, we performed
65 GWAS on a cohort of approximately 100 extensively characterized inbred mouse strains, known
66 as the hybrid mouse diversity panel (HMDP) (Ghazalpour et al. 2012). This robust resource
67 enables the investigation of both genetic and environmental influences on intricate traits. Our study
68 successfully identified distinct genetic and phenotypic differences, expanding upon the known
69 Mendelian ARHL genes (Ahl) described to date (Lavinsky et al. 2015; Ohmen et al. 2014). The
70 mouse model provides a valuable platform for studying the genetics of hearing loss, as the mouse
71 and human ears are functionally and genetically homologous, allowing for the translation of
72 findings to human populations (Ghazalpour et al. 2012; Flint and Eskin 2012; Rau et al. 2015).
73 However, additional studies are required to fully understand how the identified variants influence
74 the ARHL phenotype. The loss of cochlear HCs and their associated mechanoelectrical
75 transduction function significantly contributes to the development of ARHL (Schuknecht and
76 Gacek 1993). HCs, specialized sensory cells within the inner ear, possess stereocilia, tiny hair-like
77 structures arranged in a staircase pattern. Each stereocilium consists of a bundle of actin filaments,
78 tightly regulated in length, and anchored at their base, into a cuticular plate that consists of dense
79 actin meshwork. Actin-regulatory proteins play a crucial role in maintaining the fine actin structure,

80 and mutations in these proteins have been associated with various forms of hereditary hearing loss
81 (Miyoshi et al 2021). However, the precise role of actin-regulatory proteins in ARHL remains
82 unclear. Rho-GTPases, such as cell division cycle 42 (Cdc42) and RhoA, are well-known actin-
83 regulatory proteins that play a pivotal role in regulating actin dynamics in HCs (Ueyama et al 2014;
84 Anttonen et al. 2017). Formin proteins that function as downstream effectors of RhoA are involved
85 in regulating multiple cellular actin cytoskeletal elements by nucleating and polymerizing straight
86 actin filaments (Breitsprecher and Goode 2013). While the Diaphanousrelated formin family
87 (DRF) members DIAPH1 (Lynch et al. 1997) and DIAPH3 (Sánchez-Martínez et al. 2017; Schoen
88 et al. 2010) are known hereditary hearing loss-related proteins, the physiological role of other DRF
89 proteins in the HC, such as FHOD, have yet to be fully established.

90 FHOD3, initially described in the regulation of sarcomere organization in cardiomyocytes, has
91 been localized to thin actin filaments with abundant expression in both myocardium and skeletal
92 muscle (Taniguchi et al. 2009). Depletion of FHOD3 leads to a reduction of filamentous actin and
93 disruption of sarcomere organization in cardiac cells (Taniguchi et al. 2009). Studies have shown
94 that FHOD3 is involved in actin polymerization and myofibril integrity (Kan-o et al. 2012).
95 Interestingly, FHOD3 has been observed at the pointed ends of actin filaments, where
96 depolymerization normally occurs, suggesting a potential role in annealing short actin filaments
97 (Fujimoto et al. 2016).
98 In this study, we aimed to investigate the functional implications of Fhod3, a novel candidate gene
99 for ARHL identified through meta-analysis GWAS in mice. We generated two mouse models:
100 Fhod3 overexpression mice (*Fhod3*$^{Tg/+}$*; Pax2-Cre*$^{+/-}$) and HC-specific conditional knockout mice
101 (*Fhod3*$^{fl/fl}$*; Atoh1-Cre*$^{+/-}$) to assess the effects fluctuation in FHOD3 levels on the functioning of
102 inner ear with audiological assessments in the transgenic mice revealing a progressive high-

103 frequency hearing loss phenotype, accompanied by the predominant loss of outer HCs and
104 deterioration of the cuticular plate. Scanning electron microscopy analysis demonstrated shortened
105 stereocilia, particularly in the mid-base and base regions of the cochlea. Furthermore, targeted
106 deletion of Fhod3 replicated the progressive hearing loss and HC deterioration observed in the
107 Fhod3 overexpression mutants. These findings suggest a critical role for Fhod3 in regulating actin
108 dynamics in the cuticular plate and stereocilia of high frequency cochlear hair cells.
109

110 **2. Results**

111

112 **2.1 Random effects meta-analysis GWAS identifies 5 loci for ARHL in mice**

113 Mouse strains exhibit higher heritability for complex traits, and the genetic loci associated with
114 these traits tend to exert stronger effects compared to humans. Motivated by these advantages, we
115 performed the first GWAS of its kind in the mouse by combining several data sets in a metaanalysis
116 to identify loci associated with ARHL (Ohmen et al. 2014). We identified five genomewide
117 significant loci ($P<1.0\text{x}10^{-6}$). One of these confirmed a previously identified locus (*Ahl8*) on distal
118 chromosome 11 and greatly narrowed the candidate region. Another locus of interest appeared for
119 the 32 kHz tone burst stimulus and localized to chromosome 18 with the peak SNP
120 (position 24320393; $P=2.32 \text{ x } 10^{-6}$) appearing within a haplotype block between 24.25 and 25.65
121 Mb containing the formin-like gene *Fhod3* (Ohmen et al. 2014). Due to its role in actin
122 polymerization/capping, we decided to delve into the potential role of *Fhod3* in high-frequency
123 and progressive hearing loss.
124

125 **2.2 Spatial expression patterns of Fhod3 mRNA and protein in the cochlea.**

126 To analyze the gene expression patterns of Fhod3 in the inner ear, we employed multiplexed error-
127 robust fluorescence in situ hybridization (MERFISH) (Chen et al. 2015) in P5 cochlea. The
128 application of single-molecule imaging allowed us to visualize Fhod3 expression in auditory HCs
129 and SGNs of the cochlea with high resolution (Fig. 1A to C). Additionally, we conducted
130 immunofluorescence staining in P5 cochleae to further confirm the localization of Fhod3. Our
131 results revealed the expression of Fhod3 in both outer HCs (OHCs), inner HCs (IHCs), and in
132 SGNs (Fig. 1C). We generated a conditional knock-out mouse model targeting Fhod3 specifically
133 in HCs using Atoh1-cre and Fhod3-flox mice. In these knock-out mice ($Fhod3^{fl/fl}$; $Atoh1\text{-}Cre^{+/-}$),
134 Fhod3 signals were absent in HCs but still observed in SGNs, verifying Fhod3 expression in the
135 cochlea (Fig.1C). Furthermore, to gain insights into the subcellular localization of Fhod3 within
136 HCs, we developed an Fhod3-HA tagged knock-in mouse model ($Fhod3^{HA/+}$) in which a 3xHA
137 sequence was inserted into the C-terminus of Fhod3 prior to the stop codon. This demonstrated
138 that Fhod3 predominantly localized to the cuticular plate in HCs (Fig.1D and E). Supporting these
139 findings, data obtained from gEAR.org (https://umgear.org/) corroborates the high enrichment of
140 Fhod3 expression specifically in cochlear HCs.

141

142 **2.3 Generation of a transgenic mouse model overexpressing Fhod3**

143 In our meta-analysis GWAS, the largest sample set utilized backcross data with C57/Bl6 (B6) and
144 DBA/2J (D2) strains to map *Ahl8* (Ohmen et al. 2014). Considering the hearing effect observed in
145 our meta-analysis, we aimed to investigate the potential differential expression of *Fhod3* as a
146 plausible mechanism. Through quantitative PCR (qPCR) analysis, we found significantly higher
147 levels of Fhod3 mRNA in D2 cochleae, a model of early-onset progressive hearing loss (B6 vs
148 D2; 1.07 ± 0.088 vs 2.00 ± 0.643, p^{**}=0.0079 by Mann-Whitney U test) (Fig. 2A). These findings

149 led us to hypothesize that *Fhod3* expression variation might contribute to hearing loss. To further
150 explore this hypothesis, we sequenced the *Fhod3* clone obtained from B6 cochleae and identified
151 three missense mutations (A1888C/rs29670988, C2232T/rs13483257, and G2730A/rs30077504)
152 as well as four synonymous polymorphisms in the D2 allele (Fig.2B). Although the coding
153 variations in the D2 allele were not predicted to be deleterious by PolyPhen and SIFT software,
154 we postulated that the hearing loss phenotype could still be associated with this region, possibly
155 due to *Fhod3* overexpression in D2. To investigate this possibility, we generated a transgenic
156 mouse model by introducing the full-length Fhod3 cloned from B6 cochleae between loxP-flanked
157 stop cassettes and IRES-GFP, allowing tissue-specific Fhod3 overexpression in vivo (Fig.2C).
158 Two transgenic mouse lines were obtained and subsequently crossed with a B6 Pax2-Cre driver
159 line (Ohyama and Groves 2004) to induce Fhod3 overexpression in the developing inner ear
160 epithelium. The resulting offspring carrying both the *Fhod3* allele and *Pax2-Cre* genes (*Pax2-*
161 *Cre*$^{+/-}$*; Fhod3*$^{Tg/+}$) exhibited normal survival and did not display any gross morphological
162 phenotype. Through qPCR and immunofluorescence, we observed elevated levels of Fhod3
163 mRNA (WT vs TG; 1.00 ± 0.311 vs 5.84 ± 0.821, p^{**}=0.0095 by Mann-Whitney U test) (Fig. 2D)
164 and of FHOD3 protein expression in the mutant cochlea (Fig. 2E).
165

166 **2.4 Inner ear specific *Fhod3* overexpression leads to progressive high-frequency hearing**
167 **loss with outer hair cell dominant HC loss and cuticular plate deterioration.**

168 To assess the auditory function of the Fhod3 transgenic mice (*Fhod3*$^{Tg/+}$*; Pax2-Cre*$^{+/-}$), auditory
169 brainstem responses (ABR) were measured at 6 and 12 weeks postnatally. The mutant mice
170 demonstrated a progressive elevation of ABR thresholds specifically at 24 kHz and 32 kHz
171 frequencies [WT vs TG: (6 weeks) 26.7 ± 1.47 vs 38.3 ± 6.91 dB at 24kHz, p= 0.0097, 42.1 ± 7.72

172 vs 64.6 ± 3.97 at 32 kHz, p<0.0001; (12 weeks) 25.0 ± 1.01 vs 46.25 ± 5.99 dB at 24 kHz, p<0.0001,
173 42.9 ± 5.28 vs 75.4 ± 2.13 dB at 32 kHz, p<0.0001] (Fig. 3A). Corresponding to the threshold
174 elevation, histological examination revealed HC loss predominantly in the OHCs within the region
175 associated with high frequencies at 5 months old (Fig. 3B). The OHC survival rate in the TG mice
176 was significantly decreased at the basal turn region compared to WT mice
177 (WT vs TG (%): (IHC)100 vs 100 at apical turn (Api), 98.7 ± 0.95 vs 97.7 ± 1.51 at middle turn
178 (Mid), 94.7 ± 2.24 vs 85.9 ± 6.90 at basal turn (Base); (OHC) 97.1 ± 1.16 vs 95 ± 2.56 at Api,
179 96.8 ± 0.36 vs 96.5 ± 1.42 at Mid, 95.6 ± 0.64 vs 75.93 ± 8.98 at base, p^*=0.0233 by two-way
180 ANOVA followed by a Tukey post-hoc test) (Fig. 3C). Additionally, a significant reduction in
181 phalloidin intensity at the cuticular plate, a critical structure composed of a dense actin meshwork,
182 was observed in OHCs at the mid-basal turn (WT vs TG: (IHC)1.00 ± 0.175 vs 0.92 ± 0.179;
183 (OHC)1.00 ± 0.131 vs 0.70 ± 0.170, p^{***}<0.001, by Mann-Whitney U test). (Fig. 3D and E).
184 These findings strongly suggest that increased Fhod3 expression reduces HC integrity, leading to
185 progressive hearing loss through HC loss.
186

187 **2.5 FHOD3 overexpression deteriorated the third row of stereocilia of the hair cells in**
188 **the base of the cochlea.**

189 To investigate the impact of Fhod3 overexpression on stereocilia, we conducted an ultrastructural
190 analysis using scanning electron microscopy on transgenic mice (TG) (*Fhod3*$^{Tg/+}$*; Pax2-Cre*$^{+/-}$) in
191 comparison to wild-type mice (WT) (*Fhod3*$^{Tg/+}$*; Pax2-Cre*$^{-/-}$) at 7 weeks of age. Our examination

192 revealed a significant decrease in the number of stereocilia in the shortest (third) row of both inner
193 and outer hair cells within the basal regions of the cochlea in the TG mice (Fig. 4). These findings,
194 combined with our localization data demonstrating Fhod3 presence in the cuticular plate (Fig. 1E
195 and F), indicate that FHOD3 plays a crucial role in maintaining actin dynamics within the
196 stereocilia of both IHCs and OHCs via the cuticular plate.
197

198 **2.6 Targeted deletion of *Fhod3* induced progressive hearing loss and hair-cell**
199 **deterioration.**

200 Constitutive knockout of Fhod3 in mice results in prenatal lethality, likely due to developmental
201 defects in the myocardium (Kan-o et al. 2012). Therefore, to gain deeper insights into the specific
202 impact of Fhod3 deficiency on the mouse cochlea, it was crucial to achieve tissue specific
203 inactivation of Fhod3. To accomplish this, we generated mice with a floxed allele of Fhod3
204 combined with a Atoh1 promoter-driven Cre construct, enabling HC-specific Fhod3 inactivation.
205 Remarkably, these mutant mice exhibited a physiological phenotype similar to that of Fhod3
206 overexpression mutants, characterized by elevated auditory brainstem response (ABR) thresholds
207 specifically at the highest frequencies of 24 kHz and 32 kHz [WT vs KO: (6 weeks) 34.25 ± 4.12
208 vs 36.2 ± 2.83 dB at 24kHz, 36.3 ± 5.03 vs 50.1 ± 6.35 at 32 kHz, p^{**}=0.0096; (12 weeks) 32.3 ±
209 1.20 vs 52.9 ± 5.80 dB at 24 kHz, p^{**}=0.0031, 39.0 ± 4.51 vs 73.5 ± 4.55 dB at
210 32 kHz, p^{***}<0.0001; (18 weeks) 34.9 ± 2.93 vs 53.8 ± 3.06 dB at 24kHz, p^{*}= 0.0187, 51.4 ±
211 4.91 vs 80.8 ± 3.74 at 32 kHz, p^{***}<0.0001] (Fig. 5A). Importantly, the observed high frequency
212 hearing loss progressed over time and heterozygous (Het) mice also showed threshold elevation in
213 the high frequency. [Het: (6 weeks) 41.8 ± 6.53 dB at 24kHz, 54.3 ± 5.43 at 32 kHz, p^{*}=0.0179
214 (vs WT); (12 weeks) 47.0 ± 9.42 dB at 24 kHz, 72.4 ± 6.29 dB at 32 kHz, p^{***}<0.0001 (vs WT);

215 (18 weeks) 67.3 ± 13.6 dB at 24kHz, p^{***}= 0.0002 (vs WT), 86.0 ± 4.86 at 32 kHz,
216 p^{***}<0.0001(vs WT)]. Additionally, we observed a significant increase in hair cell loss in the
217 basal turn of the cochlea at 3 months of age in KO mice (Fig. 5B), along with a notable reduction
218 in phalloidin intensity in IHCs and OHCs at the cuticular plate in the mid-basal turn of the cochlea
219 (WT vs KO: (IHC)1.00 ± 0.037 vs 0.96 ± 0.005, p^{*}=0.035; (OHC)1.00 ±

220 0.023 vs 0.67 ± 0.017, p^{***}<0.001 by Mann-Whitney U test) (Fig. 5C), consistent with our
221 findings in the transgenic overexpression mice (Fig. 3E). Scanning electron microscopy analysis
222 similarly revealed fused, shortened, and missing stereocilia in the mid-base of the cochlea,
223 corresponding to the tonotopic region associated with hearing loss (Fig. 5E). These results indicate
224 that alterations in Fhod3 expression levels, whether elevated or reduced, disrupt the stoichiometry
225 of actin polymerization at the cuticular plate, primarily affecting the HCs of the third row
226 stereocilia in the mid-basal and basal regions of the cochlea.
227

228 **3. Discussion**

229 Here we provide compelling evidence for the crucial role of Fhod3, identified through a meta-
230 analysis of GWAS for age-related hearing loss (ARHL), in maintaining auditory function. Using
231 genetic and molecular approaches, we demonstrated that altered expression of Fhod3 leads to
232 progressive high-frequency dominant hearing loss in two different mouse models: *Pax2-Cre*$^{+/-}$;
233 *Fhod3*$^{Tg/+}$ and *Atoh1-Cre*$^{+/-}$; *Fhod3*$^{fl/fl}$. Moreover, we observed the deterioration of the cuticular
234 plate and the shortest row of stereocilia in the mutant mice, indicating that dysregulation of Fhod3
235 disrupts actin turnover balance and affects the integrity of cochlear HCs. This disruption results in
236 the loss of OHCs and could be a potential mechanism underlying ARHL.
237

238 In our previous meta-analysis GWAS, which mainly involved C57BL/6J (B6) and DBA/2J (D2)
239 F1 intercross data, we identified five genome-wide significant loci associated with ARHL in mice
240 (Ohmen et al. 2014). In this study, we focused on investigating the potential involvement of Fhod3
241 in high-frequency and progressive hearing loss, despite the presence of several other candidate
242 genes within the 1Mb interval of the haplotype block. Although we did not find deleterious Fhod3
243 polymorphisms in the D2 strain (Fig.2B), quantitative PCR revealed significantly higher inner ear
244 expression of Fhod3 in D2 compared to B6 (Fig.2A). Furthermore, Fhod3 mRNA was detected in
245 the human inner ear transcriptome (Schrauwen et al. 2016), supporting its role in human hearing.
246 We subsequently demonstrated that overexpression of Fhod3 in the inner ear leads to high-
247 frequency hearing loss in transgenic mice, accompanied by sparse actin meshwork in the cuticular
248 plate and loss of the shortest row of stereocilia in specific cochlear turn. Notably, mice with P264L
249 gamma actin mutations exhibited a similar phenotype of stereocilia loss (Drummond et al. 2012).
250 While mutations in Fascin Actin-Bundling Protein 2 (Fscn2) were implicated in mid-high
251 frequency hearing loss in D2 mice, they did not account for the complete D2 phenotype, including
252 higher frequency loss and disruption of stereocilia third row in OHCs (Shin et al. 2010). These
253 observations collectively indicate that Fhod3 plays a pivotal role in high-frequency auditory
254 function.
255 Other formin proteins have been associated with hereditary hearing loss, suggesting that altered
256 expression of Fhod3 in our mutant mouse models may contribute to the underlying molecular
257 mechanisms of hearing loss. Mutations in two formin-related hearing loss genes, DIAPH1 and
258 DIAPH3, are predicted to result in a gain-of-function mechanism (Schoen et al. 2010; Ueyama et
259 al. 2016). In line with this, our Fhod3 overexpression mouse model exhibited progressive hearing
260 loss and dominant loss of OHCs in the basal turn region, resembling the DIAPH1 transgenic mice
261 model (Ueyama et al. 2016; Ninoyu et al. 2020). Considering the subcellular localization of Fhod3

262 primarily in the cuticular plate, and similar phenotypes between loss and overexpression of Fhod3
263 leading to defective stereocilia bundle structures, we speculate that Fhod3 expression must be
264 tightly modulated to preserve normal cuticular plate and stereocilia structure. The high frequency
265 range of hearing is particularly susceptible to damage due to its greater mechanical demands but
266 may perhaps also be more generally susceptible to accumulated age-related damage due to higher
267 metabolic requirements (Someya et al. 2010). Significantly, targeted deletion of Fhod3 in
268 conditional knockout mice resulted in a similar phenotype, characterized by elevated ABR
269 thresholds and stereocilia deterioration in the mid-base and base of the cochlea. Even heterozygous
270 mice exhibited progressive hearing loss in the high-frequency range, indicating a dose-dependent
271 effect of Fhod3 expression. Indeed, a Fhod3 variant with a missense mutation at a conserved
272 residue in the FH2 domain (Tyr1249A) causes dilated cardiomyopathy by impairing the ability to
273 induce actin dynamics-dependent activation of the transcription factor serum response factor
274 (SRF) (Arimura et al. 2013). These findings are consistent with a critical role for Fhod3 in
275 maintaining actin stoichiometry in the cuticular plate and stereocilia.
276
277 Overall, our study highlights the importance of Fhod3 in regulating actin dynamics and its critical
278 role in maintaining the structural integrity of HCs in the cochlea. These findings provide valuable
279 insights into the pathogenesis of ARHL and open up potential avenues for therapeutic interventions.
280 Further investigations into the molecular mechanisms underlying Fhod3-mediated actin
281 polymerization and its interaction with other proteins involved in hearing loss will deepen our
282 understanding of the disease and pave the way for targeted therapeutic strategies.
283
284

285 **4 Material and Methods**

286 **4.1 Animals**

287 All animal protocols were approved (s17178) by the Institutional Care and Use Committee
288 (IACUC) at University of California San Diego (UC San Diego). C57BL/6J and CBA/J mice used
289 in this study were purchased from Jackson Laboratory (ME, USA).

290 **4.2 Establish Fhod3 over-expression mouse model**

291 We generated a transgenic (TG) mouse model of Fhod3 expressing CAG-loxP-STOP-
292 loxP(LSL)mouse Fhod3-IRES-GFP. Cochlear RNA was extracted from C57BL/6J mouse with
293 Micro Scale RNA isolation Kit (Ambion) according to the manufacturer's instructions, followed
294 by cDNA synthesis using ProtoScript® Taq RT-PCR Kit [New England Biolabs (NEB), Ipswich,
295 MA, USA].
296 *Fhod3* cDNA was amplified with PrimeSTAR® GXL DNA Polymerase (R050B; Takara Bio, San
297 Jose, CA, USA) using a pair of primers (5'-CACCATGGCCACGCTGGCTTGTCGCGTGCAG3'
298 for the forward and 5'-GAGCATGCTCACAGTTGCAGTTCAGATGTG -3' for the reverse
299 primer), and subcloned into the pENTR™/D-TOPO™ vector (K2400-20; Thermo Fischer
300 Scientific, Waltham, MA, USA). For the general donor vector, a pair primer (5'-
301 TGCAGGATCCATCGATCACCATGGCCACGCTGGCTTGTCGCGTGCAG-3' for the
302 forward and 5'- CGAGCTCGTCGACGATTCACAGTTGCAGTTCAGATGTG-3' for the

303 reverse primer) was utilized for amplifying *Fhod3* cDNA from the plasmid and this 4.7kb fragment
304 was subsequently cloned into a pGreen-RAGE vector cut with EcoR-V, which includes a
305 CMV/Beta actin Promoter-LSL-MCS-IRES-GFP, by using Gibson Assembly® Cloning Kit (NEB,

306 USA). After confirming the identity of the plasmid by sequencing, the linearized construct was
307 electroporated into mouse embryonic stem cells (mESCs) with a C57BL/6 background.
308 Genotyping was performed using the following primer set; 5'-TGCAGGATCCATCGATCACC3'
309 and 5'-AACTTCGACCCAACGAGC-3'. Fhod3-overexpression mice were generated by crossing
310 *Tg(Pax2-cre)1Akg/Mmnc* mice(Ohyama and Groves 2004) with the *Fhod3*$^{Tg/+}$.
311

312 **4.3 Generation of hair-cell specific Fhod3 conditional knock-out mouse**

313 HC specific Fhod3 conditional knockout mice (KO) were generated by crossing B6.Cg-
314 *Tg(Atoh1cre)1Bfri/J* mice (The Jackson Laboratory, stock no. 011104) with Fhod3$^{fl/fl}$ mice
315 (Accession No. [CDB0927K]: http://www2.clst.riken.jp/arg/mutant%20mice%20list.html) which
316 was generated as previously described (Ushijima T et al. 2018). The Fhod3$^{fl/fl}$ mice contain loxP
317 sites flanking exon 18 of the *Fhod3* gene.

318 **4.4 Generation of Fhod3-HA knock-in mice**

319 Using CRISPR/Cas9 editing we generated Fhod3-HA fusion knock-in mice expressing three
320 copies of the human influenza hemagglutinin (HA; TACCCGTATGATGTTCCGGATTACGCT)
321 tag sequence integrated at the C-terminus of Fhod3. Geneious Prime software (Biomatters,
322 Auckland, New Zealand) was utilized to identify the following guide RNA (gRNA) sequences:

323 GCAGTTCAGATGTGCCAACC was located on the last coding exon (exon 28) and
324 GCTGAGCAGAGGACCAGATC was located on the Fhod3 3' untranslated region (3'UTR). For
325 homology-directed repair (HDR), a 1,879 base-pair Fhod3 donor fragment was amplified from
326 mouse genomic DNA by using the following primers (5'-
327 GCCCATAGGAGGGCCTTTACATTTAGTTTTG-3'and 5'-
328 CAGGTGCCTAGAAAGTGACTTAGATTTCCAGG-3'), and cloned into a custom mini-circle
329 compatible hybrid donor plasmid consisting of two U6 promoters (one for each guide) and a
330 docking site for the homology arms and HA tag as previously described (Jurlina et al. 2022).
331 Integration of the amplified mouse genomic DNA into the donor plasmid and integration of the 3x
332 HA tag before the stop codon were each carried out by Gibson assembly (NEB, USA). HDR into
333 C57BL/6J background mouse embryos was carried out by mixing the plasmid donor, guide RNAs
334 [Integrated DNA Technologies (IDT), IA, USA] and Cas9 protein (Alt-R® S.p. HiFi Cas9
335 Nuclease V3; IDT, USA) together and microinjecting into mouse embryos with. For mouse
336 genotyping, following a primer set was used; 5'-GCTTTCCACATAGCACCTACA-3' and 5'-
337 CAGATGTTCAGGTCAAGTCTCC-3'.
338

339 **4.5 Immunofluorescence staining**

340 Mice were anesthetized using an intraperitoneal injection of an anesthetic cocktail (ketamine
341 92.5mg/kg, xylazine 10 mg/kg, and acepromazine 1.85 mg/kg) and fixed via transcardial
342 perfusion with 4% paraformaldehyde (PFA) in 0.1 M phosphate-buffered saline (PBS) (pH 7.4).
343 The cochleae were harvested and post-fixed overnight at 4 °C in 4% PFA in 0.1 M PBS (pH 7.4).
344 After fixation, the cochleae were dissected, and surface preparation was performed. The dissected

345 tissues were permeabilized in PBS with 0.3 % PBST (PBS with 0.3% Triton-X) for 30 min at room
346 temperature, followed by blocking with 10 % normal goat serum (NGS) in 0.03 % PBST for 1 h
347 at room temperature with agitation. Primary antibodies (see below) were applied to the samples in
348 0.03% PBST with 3% NGS and incubated overnight at 4 °C. After washing three times with 0.03%
349 PBST for 10 min each, the tissues were incubated with secondary antibodies in 0.03% PBST with
350 3% NGS for 1 h at room temperature with agitation. The stained tissue was briefly washed with
351 0.03% PBST and mounted in ProLong Antifade (Thermo Fisher Scientific, Cat#P36970, Carlsbad,
352 CA, USA) with a coverslip. Imaging was performed using a confocal microscope with airy-scan
353 processing (LSM880; Carl Zeiss, Jena, Germany).
354 For cryo-sectioning, the fixed cochleae were decalcified in 0.12 M ethylenediaminetetraacetic
355 acid (EDTA) at 4°C for 48 h, followed by cry protection in 30% sucrose at 4°C overnight. The
356 samples were then embedded in O.C.T. compound (Sakura Finetek, CA, USA) and cryo-sectioned
357 into 10 μm thick slices using a cryostat (CM1860; Leica Biosystems, Nussloch, Germany), The
358 sections were mounted on glass slides, and immunofluorescence staining was performed on the
359 glass slide using a hydrophobic barrier pen (IHC World, Cat# SPM0928, MD, USA), as described
360 above.
361
362 **4.6 Antibodies**

365 The following antibodies were used (polyclonal unless indicated): Fhod3 (Thermo Fisher
366 Scientific, Cat# PA5-23313, 1:100); Myo6 (Proteus Bioscience, Cat# 25-6791, 1:250); anti-HA
367 tag (Abcam, Cat# ab9110, 1:100); TuJ-1 monoclonal (R&D systems, Cat# MAB1195, 1:500);
368 Alexa Fluor 568 conjugated phalloidin (Thermo Fischer Scientific, A12380, 1:250); 4'6369
diamidino-2-phenylindole (DAPI) (Novus Biologicals, Cat# NBP2-31156, 1:50,000); Alexa Fluor
370 647-conjugated anti-mouse IgG2a (Thermo Fischer Scientific, Cat# A-21241, 1:500); Alexa Fluor
371 488-conjugated anti-rabbit IgG (Themo Fischer Scientific, Cat# A-11008, 1:500).

372 **4.7 Multiplexed error-robust fluorescence *in situ* hybridization (MERFISH)**

373

374 Samples were prepared following the manufacturer's instructions (Vizgen, Cambridge, MA, USA).
375 Briefly, cochleae from postnatal day 5 (P5) C57Bl/6J mice were fixed and cryo-sectioned into 10
376 μm thick slices as described above. RNase inhibitor (NEB, Cat# M0314L, USA) was used to
377 preserve RNA integrity during the dehydration step. The cryosections were placed onto
378 MERSCOPE slide glass (Vizgen, Cat# 20400001, MA, USA) and permeabilized in 70% ethanol
379 at 4 ℃ for 24 hours. Tissues were then incubated with blocking solution (Vizgen, Cat# 20300012,
380 USA) containing cell-boundary staining antibodies (Vizgen, Cat# 20300010 and 20300011, USA)
381 for 1 hour at room temperature. Subsequently, the stained samples were incubated with a
382 customized 140 gene panel mix (Vizgen, Cat# 20300006, USA) including Fhod3 and Myo7a
383 probes for 36 hours at 37 ℃ in a humidified cell culture incubator. After post-encoding

384 hybridization samples were washed with formamide wash buffer (Vizgen, Cat# 20300002, USA),

385 embedded in a polyacrylamide gel incubated with digestion premix (Vizgen, Cat# 20300005, 386 USA), and incubated with clearing premix (Vizgen, Cat# 20300003) until tissues became

387 transparent. Images were acquired and analyzed using the MERSCOPE system (Vizgen, USA).

388 Cell-boundary staining was employed for cell segmentation parameter determination.

389

390 **4.8 Quantitative real-time PCR**

391 Cochleae were harvested at P2 and frozen in liquid nitrogen. Samples were stored at -80 ℃ until

392 following RNA extraction. RNA was isolated with Micro Scale RNA isolation kit (Ambion,

393 Austin, TX, USA) followed by reverse transcription using cDNA synthesis kit (AMIL1791;

394 Ambion, USA). Quantitative real-time PCR (qPCR) was conducted using TaqMan® probe

395 (Fhod3; Mm00614166_m1) obtained from applied biosystems. For each sample, the qPCR assay

396 was performed in triplicate and included the housekeeping gene, GAPDH, as a reference. The 397 relative transcript quantity was determined using the $2^{-\Delta\Delta Ct}$ method, with GAPDH serving as the 398 internal control (Schmittgen and Livak 2008).

399

400 **4.9 Auditory brainstem response**

401 To assess hearing of Fhod3-TG (*Pax2-Cre*$^{+/-}$*; Fhod3* $^{TG/+}$), Fhod3-het (*Atoh1-Cre*$^{+/-}$*; Fhod3*$^{fl/+}$),

402 Fhod3-KO (*Atoh1-Cre*$^{+/-}$*; Fhod3*$^{fl/fl}$) mice and littermate control WT mice, auditory brain stem

403 responses (ABRs) were conducted. Mice were anesthetized with the anesthetic cocktail (ketamine

404 92.5mg/kg, xylazine 10 mg/kg, and acepromazine 1.85 mg/kg), and placed on a heating pad

405 (HP-4M; Physitemp Instruments Inc., Clifton, NJ) regulated by a temperature controller (TCAT406 2DF; Physitemp Instruments Inc, NJ). Subcutaneous stainless-steel electrodes were positioned at

407 the vertex of the skull and the right pinna, with the ground electrode placed near the base of the

bioRxiv preprint doi: https://doi.org/10.1101/2023.07.20.549974; this version posted July 25, 2023. The copyright holder for this preprint (which was not certified by peer review) is the author/funder. All rights reserved. No reuse allowed without permission.

408 tail. Acoustic stimuli were generated using a PXI data acquisition system (PXI-1031; National
409 Instruments, Austin, TX, USA) and amplified by an SA1 speaker driver (Tucker-Davis
410 Technologies, Alachua, FL, USA). Sound stimuli were presented to the right ear via an 8-inch long
411 plastic tube attached to a custom acoustic system (Eaton-Peabody Laboratories).(Valero et al.
412 2018) ABRs were evoked using 5-msec tone pips with a 30/s presentation rate and a 0.5 msec
413 rise/fall Blackman ramp. The stimuli were delivered at sound pressure levels (SPL) ranging from
414 20 to 100 dB in 5 dB step increments, at frequencies of 4, 8, 16, 24 and 32 kHz. The responses
415 were filtered using a 0.3–3 kHz band-pass filter, amplified by 10,000 times with a P511
416 preamplifier (Grass Instruments, Astro-Med, Inc., RI, USA), and averaged over 512 responses at
417 each dB SPL. The hearing threshold was determined as the lowest sound intensity level at which
418 a recognizable or reproducible wave was observed.

419 **4.10 Quantification of hair cell survival and cuticular plate analysis**

420 The cochleae were immuno-stained with Myo6 and phalloidin, followed by imaging using a 20X
421 objective on an Airyscan confocal microscope (LSM880; Zeiss, Germany) with a pixel size of
422 49nm. Viable hair HCs labeled with Myo6 were manually counted at each cochlear turn: apical
423 (corresponding to the 6-8 kHz region), middle (corresponding to the 12-24 kHz region), and basal
424 (corresponding to the 32-42 kHz region). The survival rate was calculated as the ratio of the
425 number of Myo6-positive HCs to the total number of HCs, including depleted HCs. ImageJ
426 software (available at http://rsb.info.nih.gov/ij; developed by Wayne Rasband, National Institutes
427 of Health, Bethesda, MD, USA) was utilized for the analysis.

428 For the cuticular plate analysis, the average phalloidin intensity at the cuticular plate was measured
429 using ImageJ software. Circular regions of interest (ROIs) were defined at the cuticular plate level

bioRxiv preprint doi: https://doi.org/10.1101/2023.07.20.549974; this version posted July 25, 2023. The copyright holder for this preprint (which was not certified by peer review) is the author/funder. All rights reserved. No reuse allowed without permission.

430 adjacent to the stereocilia in outer hair cells (OHC) and inner hair cells (IHC). The same ROIs
431 were applied consistently across experiments. Relative intensity changes were calculated by
432 comparing the phalloidin intensity of the mutants with that of age-matched wildtype (WT) mice.

433 **4.11 Scanning electron microscopy**

434 All animals used in this work were handled following the NIH and UCSD Guidelines for Animal
435 Care as mentioned earlier. Mice were euthanized with CO_2 and decapitated. Inner ears were
436 immediately removed with a fine scissor, transferred to a plastic Petri dish where a small aperture
437 in the bone at the apex region was made with a needle to allow the fixative to flow throughout the
438 whole sensory epithelium. A freshly prepared fixative solution containing 4% formaldehyde
439 [Electron microscopy sciences (EMS)], 2.5% glutaraldehyde (EMS), 100 mM sodium cacodylate
440 buffer (EMS), 2 mM CaCl2 was gently injected into the round window and left for 2 h at room
441 temperature. Then, the cochleae were washed in PBS for 20 min three times, organs of Corti fine
442 dissected under a stereoscope, and transferred to 20-mL glass vials with 100 mM sodium
443 cacodylate buffer. Samples were prepared for SEM imaging by OTOT method where two
444 consecutive baths of buffered 1% osmium tetroxide (EMS) and 1% tannic acid (Sigma- Aldrich,
445 St. Louis, MO, USA) were applied for 1 h, with 10 min washes for three times in between. Samples
446 were dehydrated in a graded series of ethanol 200-proof (Thermo Fischer Scientific, USA) till
447 absolute, critical-point dried (Leica EM CPD300; Leica, Wetzlar,
448 Germany), placed on carbon tape onto aluminum stubs, gold-sputtered with ~4 nm thick (Leica
449 EM SCD500; Leica, Germany), and observed in a FEG-SEM (Zeiss Sigma VP; Zeiss,
450 Germany), operated at 5 kV.

bioRxiv preprint doi: https://doi.org/10.1101/2023.07.20.549974; this version posted July 25, 2023. The copyright holder for this preprint (which was not certified by peer review) is the author/funder. All rights reserved. No reuse allowed without permission.

4.12 Statistical analysis

All statistical analyses were performed using GraphPad Prism (Prism 9.2.0.; GraphPad Software Inc., La Jolla, CA, USA). All data were presented as mean ± standard deviation or standard error of the mean (SEM). For ABR and survival HCs analysis, two-way analysis of variance (ANOVA) was used to detect significant differences, followed by a Tukey post-hoc test. For others, MannWhitney U test was utilized. All statistical details can be found in figure legends. The results were considered statistically significant at $P < 0.05$ (*), $P < 0.01$ (**) and $P < 0.001$ (***).

5. Conflicts of Interest

The authors declare no conflict of interests

6. Acknowledgement

This study was supported by grants from National Institutes of Health (R01 DC-018566 to R.A.F.). U.M. is supported by NIDCD R21 (DC-018237), NIDCD R01 (DC021075), Core Grant NCI CCSG (CA014195), Nathan Shock Center for Aging Research at the Salk Institute P30 AG068635, and a CZI Imaging Scientist Award.

7. Authors Contribution

R.A.F and U.M. designed the experiments. E.B. and Y.N. contributed equally as first author. E.B. performed animal studies and some immunofluorescence (IF). Y.N. performed MERFISH, IF, HCs and cuticular plate analysis. E.B. and Y.N. performed all statistical analysis. Q.L. and

bioRxiv preprint doi: https://doi.org/10.1101/2023.07.20.549974; this version posted July 25, 2023. The copyright holder for this preprint (which was not certified by peer review) is the author/funder. All rights reserved. No reuse allowed without permission.

472 N.O. designed and generated the TG mice line. Y.N. and K.J.W. designed and established Fhod3-
473 HA mouse line. R.T. and H.S. designed and generated Fhod3$^{fl/fl}$ mice line. L.A. performed SEM
474 experiments. Y.N., E.B., U.M. and R.A.F. analyzed data and wrote the manuscript.

bioRxiv preprint doi: https://doi.org/10.1101/2023.07.20.549974; this version posted July 25, 2023. The copyright holder for this preprint (which was not certified by peer review) is the author/funder. All rights reserved. No reuse allowed without permission.

476

477

bioRxiv preprint doi: https://doi.org/10.1101/2023.07.20.549974; this version posted July 25, 2023. The copyright holder for this preprint (which was not certified by peer review) is the author/funder. All rights reserved. No reuse allowed without permission.

8. Reference

Anttonen T, Belevich I, Laos M, Herranen A, Jokitalo E, Brakebusch C, Pirvola U. 2017. Cytoskeletal Stability in the Auditory Organ In Vivo: RhoA Is Dispensable for Wound Healing but Essential for Hair Cell Development. *eNeuro* **4**: ENEURO.0149-17.2017.

Arimura T, Takeya R, Ishikawa T, Yamano T, Matsuo A, Tatsumi T, Nomura T, Sumimoto H, Kimura A. 2013. Dilated Cardiomyopathy-Associated *FHOD3* Variant Impairs the Ability to Induce Activation of Transcription Factor Serum Response Factor. *Circulation Journal* **77**: 2990–2996.

Benkafadar N, François F, Affortit C, Casas F, Ceccato J-C, Menardo J, Venail F, Malfroy-Camine B, Puel J-L, Wang J. 2019. ROS-Induced Activation of DNA Damage Responses Drives Senescence-Like State in Postmitotic Cochlear Cells: Implication for Hearing Preservation. *Mol Neurobiol* **56**: 5950–5969.

Breitsprecher D, Goode BL. 2013. Formins at a glance. *J Cell Sci* **126**: 1–7.

Chen KH, Boettiger AN, Moffitt JR, Wang S, Zhuang X. Spatially resolved, highly multiplexed RNA profiling in single cells. *Science* **348**:aaa6090.

Drummond MC, Belyantseva IA, Friderici KH, Friedman TB. 2012. Actin in hair cells and hearing loss. *Hearing Research* **288**: 89–99.

E Van Eyken 1, G Van Camp, E Fransen, V Topsakal, J J Hendrickx, K Demeester, P Van de Heyning, E Mäki-Torkko, S Hannula, M Sorri, et al. 2007. Contribution of the Nacetyltransferase 2 polymorphism NAT2*6A to age-related hearing impairment. *J.Med. Genet.* **44**:570-8.

Flint J, Eskin E. 2012. Genome-wide association studies in mice. *Nat Rev Genet* **13**: 807–817.

Fransen E, Bonneux S, Corneveaux JJ, Schrauwen I, Di Berardino F, White CH, Ohmen JD, Van de Heyning P, Ambrosetti U, Huentelman MJ, et al. 2015. Genome-wide association analysis demonstrates the highly polygenic character of age-related hearing impairment. *Eur J Hum Genet* **23**: 110–115.

Friedman RA, Van Laer L, Huentelman MJ, Sheth SS, Van Eyken E, Corneveaux JJ, Tembe WD, Halperin RF, Thorburn AQ, Thys S, et al. 2009. GRM7 variants confer susceptibility to age-related hearing impairment. *Hum Mol Genet* **18**: 785–796.

Fujimoto N, Kan-o M, Ushijima T, Kage Y, Tominaga R, Sumimoto H, Takeya R. 2016. Transgenic Expression of the Formin Protein Fhod3 Selectively in the Embryonic Heart: Role of Actin-Binding Activity of Fhod3 and Its Sarcomeric Localization during Myofibrillogenesis. *PLoS One* **11**: e0148472.

Gates GA, Mills JH. 2005. Presbycusis. *The Lancet* **366**: 1111–1120.

bioRxiv preprint doi: https://doi.org/10.1101/2023.07.20.549974; this version posted July 25, 2023. The copyright holder for this preprint (which was not certified by peer review) is the author/funder. All rights reserved. No reuse allowed without permission.

513 Ghazalpour A, Rau CD, Farber CR, Bennett BJ, Orozco LD, van Nas A, Pan C, Allayee H,
514 Beaven SW, Civelek M, et al. 2012. Hybrid mouse diversity panel: a panel of inbred
515 mouse strains suitable for analysis of complex genetic traits. *Mamm Genome* **23**: 680–
516 692.

517 Jurlina SL, Jones MK, Agarwal D, De La Toba DV, Kambli N, Su F, Martin HM, Anderson R,
518 Wong RM, Seid J, et al. 2022. A Tet-Inducible CRISPR Platform for High-Fidelity
519 Editing of Human Pluripotent Stem Cells. *Genes* **13**: 2363.

520 Kan-o M, Takeya R, Abe T, Kitajima N, Nishida M, Tominaga R, Kurose H, Sumimoto H.
521 2012. Mammalian formin Fhod3 plays an essential role in cardiogenesis by organizing
522 myofibrillogenesis. *Biol Open* **1**: 889–896.

523 Lavinsky J, Crow AL, Pan C, Wang J, Aaron KA, Ho MK, Li Q, Salehide P, Myint A,
524 MongesHernadez M, et al. 2015. Genome-wide association study identifies nox3 as a
525 critical gene for susceptibility to noise-induced hearing loss. *PLoS Genet* **11**: e1005094.

526 Li H, Lu M, Zhang H, Wang S, Wang F, Ma X, Liu J, Li X, Yang H, Shen H, et al. 2022.
527 Downregulation of REST in the cochlea contributes to age-related hearing loss via the
528 p53 apoptosis pathway. *Cell Death Dis* **13**: 1–14.

529 Lynch ED, Lee MK, Morrow JE, Welcsh PL, León PE, King MC. 1997. Nonsyndromic deafness
530 DFNA1 associated with mutation of a human homolog of the Drosophila gene
531 diaphanous. *Science* **278**: 1315–1318.

532 Markaryan A, Nelson EG, Hinojosa R. 2010. Major arc mitochondrial DNA deletions in
533 cytochrome c oxidase-deficient human cochlear spiral ganglion cells. *Acta*
534 *OtoLaryngologica* **130**: 780–787.

535 Menardo J, Tang Y, Ladrech S, Lenoir M, Casas F, Michel C, Bourien J, Ruel J, Rebillard G,
536 Maurice T, et al. 2012. Oxidative Stress, Inflammation, and Autophagic Stress as the Key
537 Mechanisms of Premature Age-Related Hearing Loss in SAMP8 Mouse Cochlea.
538 *Antioxidants & Redox Signaling* **16**: 263–274.

539 Miyoshi T, Belyantseva IA, Kitajiri S, Miyajima H, Nishio S, Usami S, Kim BJ, Choi BY,
540 Omori K, Shroff H, et al. 2022.Human deafness-associated variants alter the dynamics of
541 key molecules in hair cell stereocilia F-actin cores. *Hum Genet* **141**:363-382

542 Ninoyu Y, Sakaguchi H, Lin C, Suzuki T, Hirano S, Hisa Y, Saito N, Ueyama T. 2020. The
543 integrity of cochlear hair cells is established and maintained through the localization of
544 Dia1 at apical junctional complexes and stereocilia. *Cell Death & Disease* **11**: 1–15.

545 Ohmen J, Kang EY, Li X, Joo JW, Hormozdiari F, Zheng QY, Davis RC, Lusis AJ, Eskin E,
546 Friedman RA. 2014. Genome-wide association study for age-related hearing loss (AHL)
547 in the mouse: a meta-analysis. *J Assoc Res Otolaryngol* **15**: 335–352.

bioRxiv preprint doi: https://doi.org/10.1101/2023.07.20.549974; this version posted July 25, 2023. The copyright holder for this preprint (which was not certified by peer review) is the author/funder. All rights reserved. No reuse allowed without permission.

548 Ohyama T, Groves AK. 2004. Generation of Pax2-Cre mice by modification of a Pax2 bacterial
549 artificial chromosome. *genesis* **38**: 195–199.

550 Rau CD, Parks B, Wang Y, Eskin E, Simecek P, Churchill GA, Lusis AJ. 2015. High-Density
551 Genotypes of Inbred Mouse Strains: Improved Power and Precision of Association
552 Mapping. *G3 Genes|Genomes|Genetics* **5**: 2021–2026.

553 Rodríguez-de la Rosa L, Lassaletta L, Calvino M, Murillo-Cuesta S, Varela-Nieto I. 2017. The
554 Role of Insulin-Like Growth Factor 1 in the Progression of Age-Related Hearing Loss.
555 *Frontiers in Aging Neuroscience* **9**.
556 https://www.frontiersin.org/articles/10.3389/fnagi.2017.00411 (Accessed June 7, 2023).

557 Sánchez-Martínez A, Benito-Orejas JI, Tellería-Orriols JJ, Alonso-Ramos MJ. 2017. Autosomal
558 dominant auditory neuropathy and variant DIAPH3 (c.-173C>T). *Acta Otorrinolaringol*
559 *Esp (Engl Ed)* **68**: 183–185.

560 Schmittgen TD, Livak KJ. 2008. Analyzing real-time PCR data by the comparative C(T)
561 method. *Nat Protoc* **3**: 1101–1108.

562 Schoen CJ, Emery SB, Thorne MC, Ammana HR, Śliwerska E, Arnett J, Hortsch M, Hannan F,
563 Burmeister M, Lesperance MM. 2010. Increased activity of Diaphanous homolog 3
564 (DIAPH3)/diaphanous causes hearing defects in humans with auditory neuropathy and in
565 Drosophila. *Proc Natl Acad Sci U S A* **107**: 13396–13401.

566 Schrauwen I, Hasin-Brumshtein Y, Corneveaux JJ, Ohmen J, White C, Allen AN, Lusis AJ, Van
567 Camp G, Huentelman MJ, Friedman RA. 2016. A comprehensive catalogue of the coding
568 and non-coding transcripts of the human inner ear. *Hear Res* **333**: 266–274.

569 Schuknecht HF, Gacek MR. 1993. Cochlear pathology in presbycusis. *Ann Otol Rhinol Laryngol*
570 **102**: 1–16.

571 Shin J-B, Longo-Guess CM, Gagnon LH, Saylor KW, Dumont RA, Spinelli KJ, Pagana JM,
572 Wilmarth PA, David LL, Gillespie PG, et al. 2010. The R109H Variant of Fascin-2, a
573 Developmentally Regulated Actin Crosslinker in Hair-Cell Stereocilia, Underlies
574 EarlyOnset Hearing Loss of DBA/2J Mice. *J Neurosci* **30**: 9683–9694.

575 Someya S, Yu W, Hallows WC, Xu J, Vann JM, Leeuwenburgh C, Tanokura M, Denu JM,
576 Prolla TA. 2010. Sirt3 Mediates Reduction of Oxidative Damage and Prevention of
577 AgeRelated Hearing Loss under Caloric Restriction. *Cell* **143**: 802–812.

578 Sugiura S, Uchida Y, Nakashima T, Ando F, Shimokata H. 2010. The association between gene
579 polymorphisms in uncoupling proteins and hearing impairment in Japanese elderly. *Acta*
580 *Oto-Laryngologica* **130**: 487–492.

bioRxiv preprint doi: https://doi.org/10.1101/2023.07.20.549974; this version posted July 25, 2023. The copyright holder for this preprint (which was not certified by peer review) is the author/funder. All rights reserved. No reuse allowed without permission.

581 Taniguchi K, Takeya R, Suetsugu S, Kan-o M, Narusawa M, Shiose A, Tominaga R, Sumimoto
582 H. 2009. Mammalian formin fhod3 regulates actin assembly and sarcomere organization
583 in striated muscles. *J Biol Chem* **284**: 29873–29881.

584 Ueyama T, Sakaguchi H, Nakamura T, Goto A, Morioka S, Shimizu A, Nakao K, Hishikawa Y,
585 Ninoyu Y, Kassai H, et al. 2014. Maintenance of stereocilia and apical junctional
586 complexes by Cdc42 in cochlear hair cells *J Cell Sci* **127**:2040-52

587 Ueyama T, Ninoyu Y, Nishio S-Y, Miyoshi T, Torii H, Nishimura K, Sugahara K, Sakata H,
588 Thumkeo D, Sakaguchi H, et al. 2016. Constitutive activation of DIA1 (DIAPH1) via
589 Cterminal truncation causes human sensorineural hearing loss. *EMBO Mol Med* **8**: 1310–
590 1324.

591 Ushijima T, Fujimoto N, Matsuyama S, Kan-o M, Kiyonari H, Shioi G, Kage Y, Yamasaki S,
592 Takeya R, Sumimoto H. 2018. The actin-organizing formin protein Fhod3 is required for
593 postnatal development and functional maintenance of the adult heart in mice. *J Biol*
594 *Chem* **293**: 148–162.

595 Valero MD, Hancock KE, Maison SF, Liberman MC. 2018. Effects of cochlear synaptopathy on
596 middle-ear muscle reflexes in unanesthetized mice. *Hearing Research* **363**: 109–118.

597 Van Laer L, Huyghe JR, Hannula S, Van Eyken E, Stephan DA, Mäki-Torkko E, Aikio P,
598 Fransen E, Lysholm-Bernacchi A, Sorri M, et al. 2010. A genome-wide association study
599 for age-related hearing impairment in the Saami. *Eur J Hum Genet* **18**: 685–693.

600

601

602

bioRxiv preprint doi: https://doi.org/10.1101/2023.07.20.549974; this version posted July 25, 2023. The copyright holder for this preprint (which was not certified by peer review) is the author/funder. All rights reserved. No reuse allowed without permission.

603 **9. Figures**

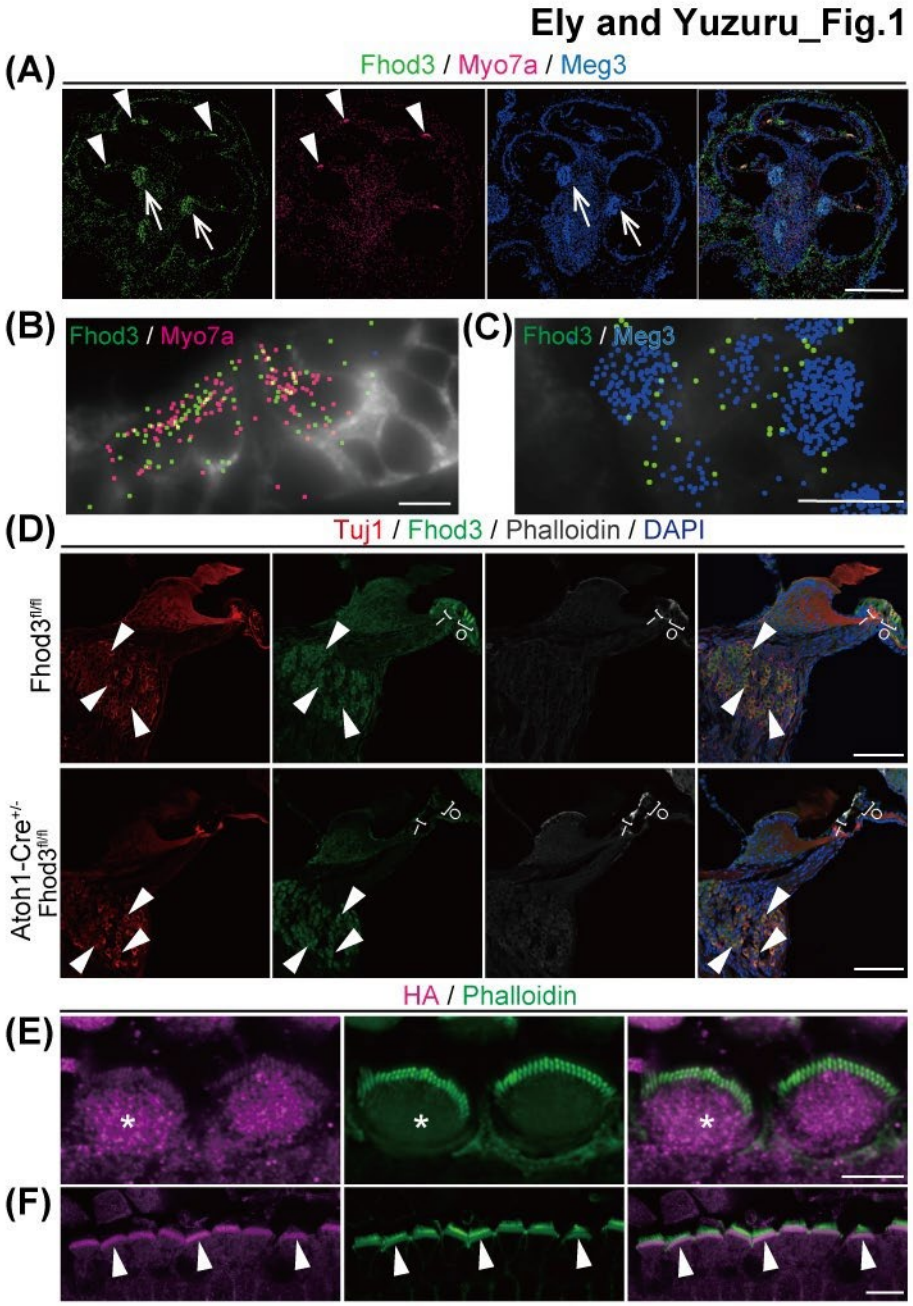

604

605

bioRxiv preprint doi: https://doi.org/10.1101/2023.07.20.549974; this version posted July 25, 2023. The copyright holder for this preprint (which was not certified by peer review) is the author/funder. All rights reserved. No reuse allowed without permission.

606 **Fig.1: Cellular and Subcellular localization of Fhod3 in the mouse cochlea**

607 Fhod3 mRNA expression in the mouse cochlea at post neonatal day 5(P5) (A-B). **A)** Multiplexed
608 error robust fluorescent in-situ hybridization (MERFISH) image of the mid modiolar section.
609 Fhod3 transcripts (green) expressed in the hair cell (HC) (arrow head) and spiral ganglion cells
610 (SGCs) (arrow). Myo7a is for HC marker (magenta) and Meg3 (dark blue) is for SGN marker.
611 Scale bar; 500μm. **B-C)** The high magnification image of organ of Corti (B) and spiral ganglion
612 cells (C) of Fig.A. Fhod3 expression was observed in both HCs and SGCs. Cell boundaries were
613 stained with cell boundary staining kit (Vizgen) and depicted by grey color. Scale bar; 25μm. **D)**
614 Cryosections of cochleae of wild type (WT) and Fhod3 knock-out (*Atoh1-Cre*$^{+/-}$*; Fhod3*$^{fl/fl}$) (KO)
615 mice at P14 were stained by Tuj1, Fhod3, phalloidin antibodies and DAPI. Fhod3 expressions
616 were observed in both HCs ant SGCs. Note that Fhod3 signals were diminished in the HC in the
617 KO mouse. Scale bar; 100μm. **E-F)** Outer HCs images at P2 in Fhod3-3xHA knock-in mouse
618 (*Fhod3*$^{HA/+}$). Cochleae were dissected and stained with anti-HA (magenta) and phalloidin (green)
619 antibodies. Fhod3 signals were mainly observed in cuticular plate (asterisk) (E). Lateral view of
620 outer hair cells and arrow heads indicate HA-positive cuticular plate (arrow head) (F). Scale bar:
621 (E) 5μm, (F) 10μm.
622

bioRxiv preprint doi: https://doi.org/10.1101/2023.07.20.549974; this version posted July 25, 2023. The copyright holder for this preprint (which was not certified by peer review) is the author/funder. All rights reserved. No reuse allowed without permission.

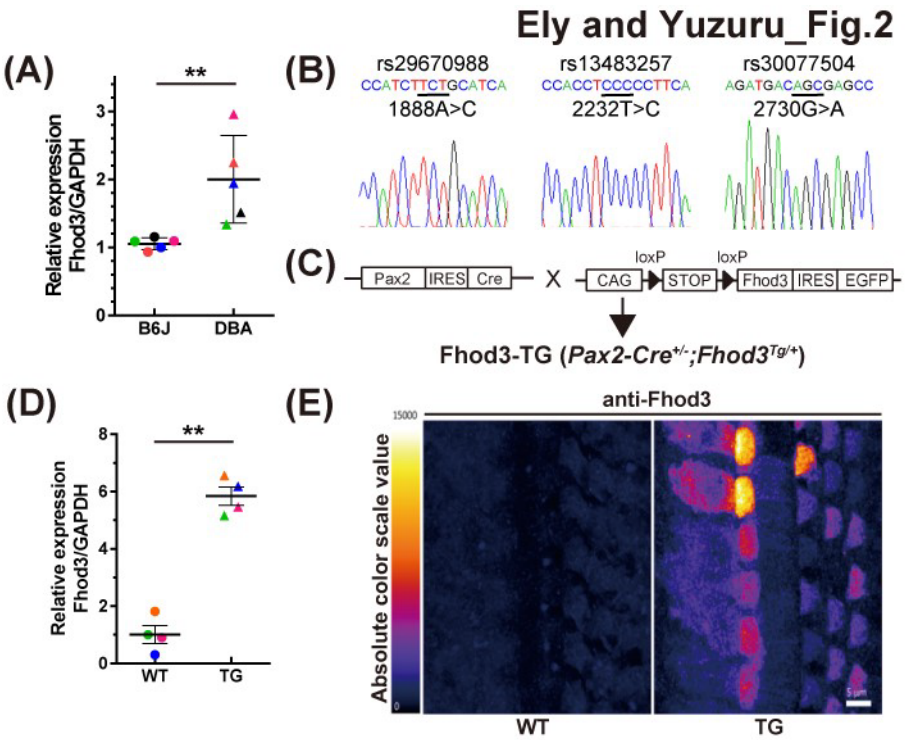

623

624

bioRxiv preprint doi: https://doi.org/10.1101/2023.07.20.549974; this version posted July 25, 2023. The copyright holder for this preprint (which was not certified by peer review) is the author/funder. All rights reserved. No reuse allowed without permission.

625 **Fig.2: Higher expression and nonsense mutations of Fhod3 in the DBA/2J mice and**
626 **generation of Fhod3 transgenic mouse**.

627 **(A)** Comparison of Fhod3 mRNA expression between C57/BL6 (B6) and DBA/2J (D2) mice.
628 Cochlear mRNA was extracted from P2 mice, and Fhod3 and GAPDH were amplified using
629 gene-specific primers. The relative expression level of Fhod3 was calculated. (n=5, Mann-
630 Whitney U test, p^{**}=0.0079).

631 **(B)** Identification of missense mutations in Fhod3 from D2 mice. A comparison of Fhod3
632 sequence cloned from B6 cochlea revealed three non-deleterious mutations: 1888A>C,
633 2232T>C, and 2730G>A. Reference SNP (rs) numbers are indicated, and changed residues
634 are underlined.

635 **(C)** Illustration of the generation of the Fhod3 overexpression mouse model. Fhod3 from B6
636 cochlea was inserted into the CMV/Beta actin Promoter-loxP-STOP-loxP-MCS-IRES-GFP
637 vector, generating a transgenic mouse overexpressing Fhod3 (TG) downstream of the
638 flanked stop codon, controlled by the CMV promoter. The TG mouse was subsequently
639 intercrossed with the Pax2-Cre mouse line to achieve cochlear-specific overexpression of
640 Fhod3 in vivo. **(D)** Relative expression of Fhod3 in wild-type B6 and TG mice. mRNA was
641 obtained from the mice cochleae at P2, and quantitative PCR was performed. Fhod3
642 expression was normalized to GAPDH. (n=4, Mann-Whitney U test, p^{**}=0.0095).

643 **(E)** Immunofluorescence intensity of Fhod3 in wild-type (WT) and TG mice at P2. The
644 glow-scale bar demonstrates the color gradient of the scale. Scale bar; 5μm.

645

bioRxiv preprint doi: https://doi.org/10.1101/2023.07.20.549974; this version posted July 25, 2023. The copyright holder for this preprint (which was not certified by peer review) is the author/funder. All rights reserved. No reuse allowed without permission.

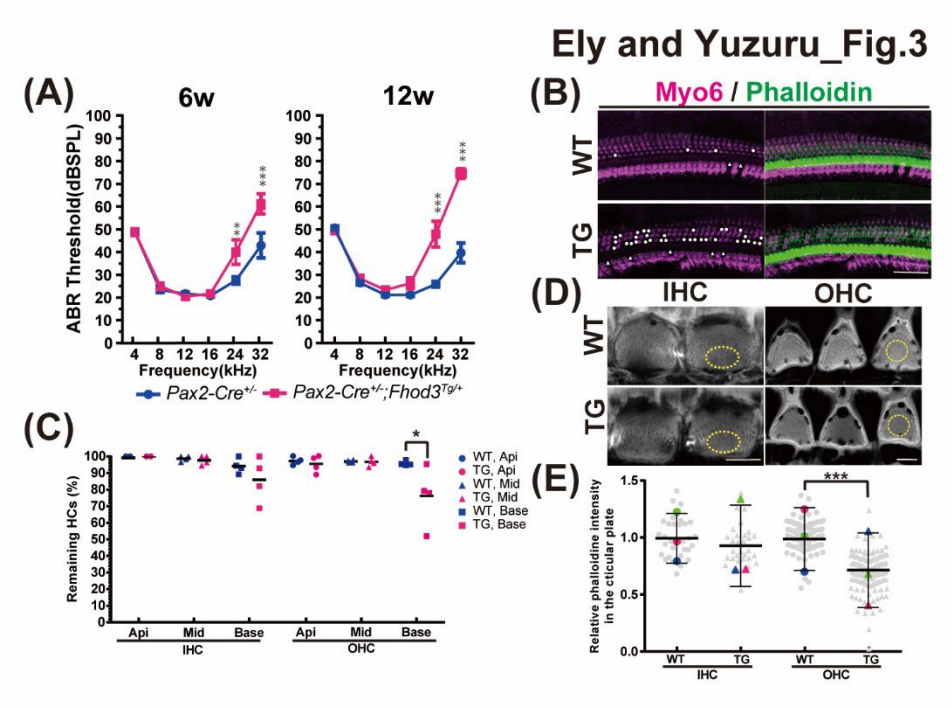

646

647

bioRxiv preprint doi: https://doi.org/10.1101/2023.07.20.549974; this version posted July 25, 2023. The copyright holder for this preprint (which was not certified by peer review) is the author/funder. All rights reserved. No reuse allowed without permission.

648 **Fig.3 Auditory phenotype and immunohistochemical analysis of Fhod3-TG mice**

649 **(A)** Auditory brainstem response (ABR) thresholds with pure-tone bursts at various
650 frequencies in WT (*Pax2-Cre*$^{-/-}$*; Fhod3*$^{Tg/+}$) and TG (*Pax2-Cre*$^{+/-}$*; Fhod3*$^{Tg/+}$) mice at 6
651 weeks and 12 weeks of age. Significant differences were observed at 24 kHz and 32 kHz,
652 and the thresholds elevation at both frequencies are progressive. Statistical analysis
653 performed using two-way ANOVA followed by a Tukey post-hoc test. (n=12 for each
654 group, p^{**}=0.0097 at 24 kHz (6 weeks), p^{***}<0.0001 at 32 kHz (6 weeks),
655 p^{***}<0.0001 at 24 kHz (12 weeks), p^{***}<0.0001 at 32 kHz (12 weeks)). **(B)**
656 Representative confocal images of the basal turn cochlea at 5 months old, showing
657 immunostaining with Myosin6 and phalloidin. White dots indicate hair cell losses. Scale
658 bar; 20μm. **(C)** Survival hair cell rate in WT and TG mice at 5 months old. The number
659 of surviving Myo6-positive inner and outer hair cells (IHCs and OHCs) was counted,
660 and the survival rate was calculated in the apical (Api), middle (Mid) and basal (Base)
661 turn cochleae. The survival rate of OHC in TG mice at the basal turn cochlea was
662 significantly decreased compared to the WT control (WT vs TG in the basal OHC (%):
663 95.6±0.64 vs 75.93±8.98, p^{*}=0.023 by Mann-Whitney U test, n=4). **(D)**
664 Immunofluorescence images in the cuticular plate of TG mice and the control at 5
665 months old. Phalloidin staining (grey) was performed and show representative images of
666 IHC and OHC in the mid-basal turn cochlea. Region of interests for the measurement of
667 phalloidin intensities are depicted by yellow color dots. Scale bar; 5μm. **(E)** Statistical
668 analysis of phalloidin staining in the cuticular plate at 5 months old. Each grey dots
669 indicates relative phalloidin intensities of remaining hair cells (total n=86, 91, 273 and
670 279), and each colored dots demonstrates average of the intensities per experiment (WT

bioRxiv preprint doi: https://doi.org/10.1101/2023.07.20.549974; this version posted July 25, 2023. The copyright holder for this preprint (which was not certified by peer review) is the author/funder. All rights reserved. No reuse allowed without permission.

vs TG: (IHC)1.00 ± 0.175 vs 0.92 ± 0.179; (OHC)1.00 ± 0.131 vs 0.70 ± 0.170, p***<0.001, by Mann-Whitney U test, n=3 animals).

bioRxiv preprint doi: https://doi.org/10.1101/2023.07.20.549974; this version posted July 25, 2023. The copyright holder for this preprint (which was not certified by peer review) is the author/funder. All rights reserved. No reuse allowed without permission.

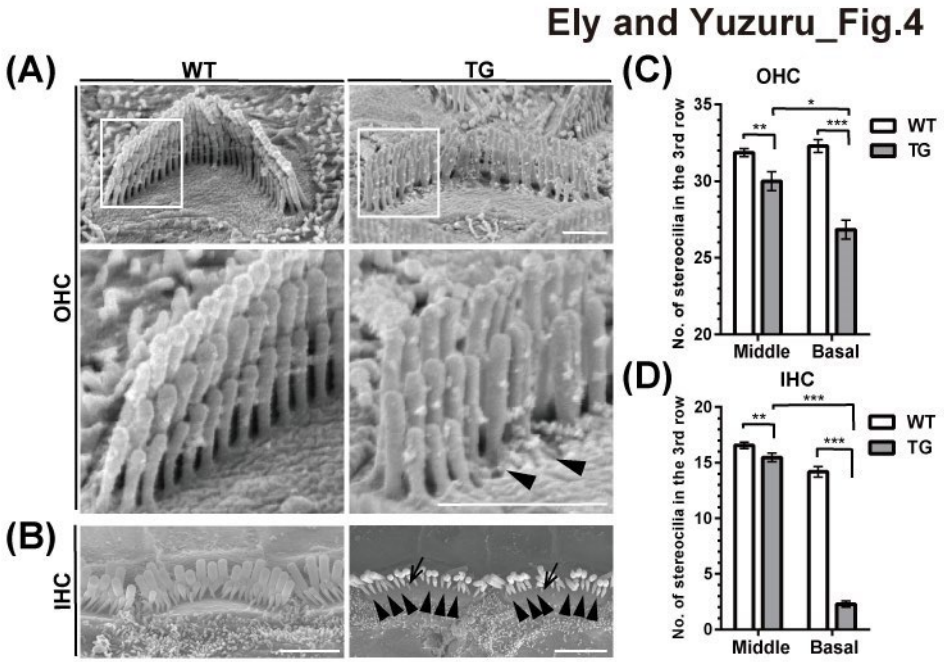

675

676 **Fig.4 Ultrastructural analysis of Fhod3 transgenic mise**

677 Scanning electron microscopy (SEM) images and the comparison of number of stereocilia in
678 the third row of 7-weeks old age cochleae. **(A) (B)** SEM images of outer hair cell (OHC)
679 (A) and inner hair cell (IHC) (B) hair cell stereocilia in WT (*Pax2-Cre*$^{-/-}$*; Fhod3*$^{Tg/+}$) and TG
680 (*Pax2-Cre*$^{+/-}$*; Fhod3*$^{Tg/+}$) mice at basal turn cochleae. White boxed regions are magnified in
681 the lower panel. Arrows indicate missing (arrowhead) and remaining (arrow) third row
682 stereocilia in the TG mice. [Scale bar; (A) 1μm, (B) 2.5μm]. **(C)(D)** Comparison of number
683 of stereocilia in the third row of OHC (C) and IHC (D) at middle and basal turn cochleae.
684 Statistical analysis was performed using Mann-Whitney U test. [(C) n=7 for the middle turn
685 (Mid) and the basal turn (Base) cochlea, p*=0.0216 at Mid, p***<0.0001 at Base; (D) n=9
686 and 11 for the Mid, n=15 for the Base, p**=0.0016 at Mid, p***<0.0001 at Base].

687

bioRxiv preprint doi: https://doi.org/10.1101/2023.07.20.549974; this version posted July 25, 2023. The copyright holder for this preprint (which was not certified by peer review) is the author/funder. All rights reserved. No reuse allowed without permission.

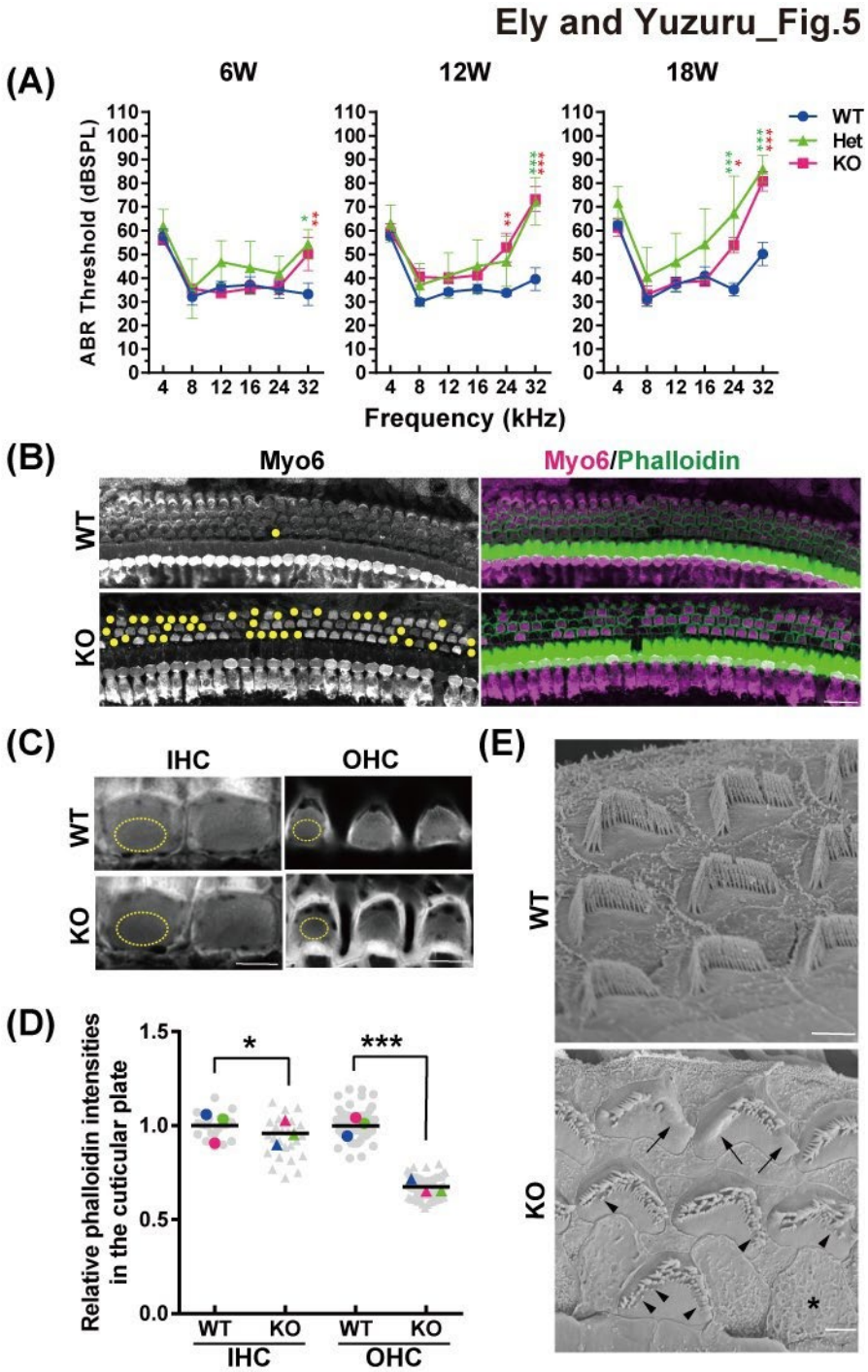

688

689

bioRxiv preprint doi: https://doi.org/10.1101/2023.07.20.549974; this version posted July 25, 2023. The copyright holder for this preprint (which was not certified by peer review) is the author/funder. All rights reserved. No reuse allowed without permission.

690 **Fig.5 Phenotypic analysis of conditional knock-out mouse of Fhod3**

691 **(A)** ABR measurements of wild type (WT) (*Math1-Cre*$^{-/-}$*; Fhod3*$^{fl/fl}$) (n=16), heterozygous
692 (Het) (*Math1-Cre*$^{+/-}$*; Fhod3*$^{fl/+}$) (n=4), knock-out (KO) (*Math1-Cre*$^{+/-}$*; Fhod3*$^{fl/fl}$) (n=9)
693 mice at 6, 12 and 18 weeks of age. Two-way ANOVA was used to detect significant
694 differences, followed by a Tukey post-hoc test. $p^{*}<0.05$, $p^{**}<0.01$, $p^{***}<0.001$.

695 **(B)** Immunohistochemical analysis was conducted on WT and KO mice cochleae from the
696 basal turn cochlea at 3 months of age. Cochleae were harvested, fixed and stained with
697 Myo6 and phalloidin. Heir cell losses were represented by yellow dots. Scale bar;20μm.

698 **(C)** Representative images of cuticular plate with phalloidin staining in WT and KO mice in
699 the mid-basal turn cochlea at 3-months old. Region of interests for the following
700 phalloidin staining analysis (D) are depicted (yellow dots). Scale bar; 5μm.

701 **(D)** Statistical analysis of phalloidin staining in the cuticular plate at 3-months old. Each
702 grey dots indicates relative phalloidin intensities of survival hair cells (total n=86, 91,
703 273 and 279), and each colored dots demonstrates average of the intensities per
704 experiment ($p^{***}<0.001$ by Mann-Whitney U test, n=3 animals).

705 **(E)** SEM images of OHC of WT and KO in the mid-basal-turn cochlea at 3-months old.
706 Abnormal fused stereocilia (arrow), short and missing stereocilia in the third row
707 (arrow head) and complete loss of stereocilia (asterisk) in KO mice are indicated. Scale
708 bar;
709 2μm.